

PAPER • OPEN ACCESS

## Analysis of nonclassical features in a coupled macroscopic binary system

To cite this article: Byoung S Ham 2020 *New J. Phys.* **22** 123043

View the [article online](#) for updates and enhancements.



## PAPER

# Analysis of nonclassical features in a coupled macroscopic binary system

## OPEN ACCESS

## RECEIVED

28 July 2020

## REVISED

14 December 2020

## ACCEPTED FOR PUBLICATION

15 December 2020

## PUBLISHED

30 December 2020

Original content from this work may be used under the terms of the [Creative Commons Attribution 4.0 licence](#).

Any further distribution of this work must maintain attribution to the author(s) and the title of the work, journal citation and DOI.

Byoung S Ham\* 

Center for Photon Information Processing, School of Electrical Engineering and Computer Science, Gwangju Institute of Science and Technology, 123 Chumdangwagi-ro, Buk-gu, Gwangju 61005, Republic of Korea

\* Author to whom any correspondence should be addressed.

E-mail: [bham@gist.ac.kr](mailto:bham@gist.ac.kr)

**Keywords:** quantum optics, quantum mechanics, coherence optics, photonic de Broglie waves, coherence de Broglie waves

Supplementary material for this article is available [online](#)

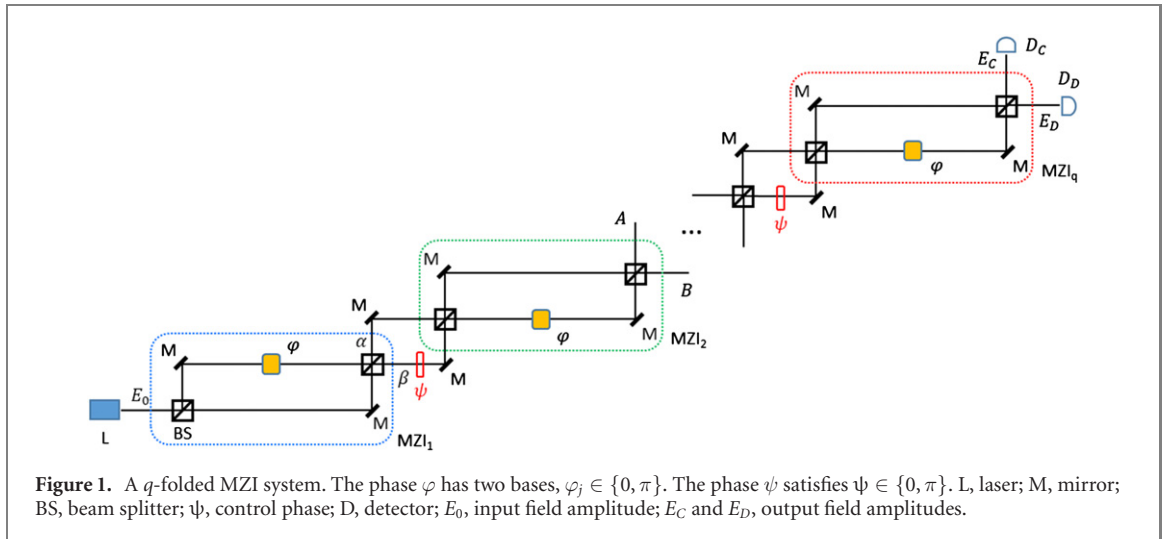
## Abstract

Nonclassical phenomena of quantum mechanics such as anticorrelation and photonic de Broglie waves (PBWs) have been recently understood as a special case of coherence optics with a particular phase relation between orthogonal bases composing a classical system. Such a macroscopic understanding of nonclassical features has also been confirmed experimentally for a coherence version of PBWs in a doubly-coupled Mach–Zehnder interferometer (MZI). Here, a multi-coupled MZI system is analyzed and discussed to obtain a general understanding of the nonclassical feature using tensor products of binary bases of a classical system. This analysis should intrigue a fundamental question on quantumness or nonclassicality limited to a microscopic world of a single photon or a single particle.

## 1. Introduction

Quantum superposition is the bedrock of not only coherence optics of interference and diffraction [1], but also quantum mechanics of nonclassical features such as anticorrelation [2–10], Franson-type nonlocal correlation [11–15], photonic de Broglie waves (PBS) [16–20], and entangled photon/spin pairs [21, 22]. A typical example of superposition is a Young’s double slit or a Mach-Zehnder interferometer (MZI), where such coherence optics has been applied for both macroscopic (coherent lights) [1] and microscopic (single particles) regimes [11–15, 23]. The key concept of quantum superposition is indistinguishability between bipartite entities in a coherence regime [24] as shown for a single photon itself via self-interference in a microscopic world [23]. For this indistinguishability, phase coherence plays a key role for quantum superposition, resulting in the uncertainty principle. Unlike the energy-time bin uncertainty relation in the microscopic world as a particle nature of quantum mechanics [2–21], a phase relation has been recently understood as the key concept of quantumness or nonclassicality [25], where such quantumness can also be induced by macroscopic coherence optics [26–29]. Here, the phase relation between bipartite entities implies the origin of the nonclassical features, where the bipartite-based quantumness can be extended into a macroscopic world such as for Schrodinger’s cat [30–35].

Recently, a novel interpretation has been applied for the Hong–Ou–Mandel (HOM) effect of photon bunching or anticorrelation to understand the fundamental physics of quantumness [25]. Unlike conventional understanding of the particle nature in quantum mechanics based on the energy-time bin relation [2–22], a simple theory of coherence optics has been successful to induce the same results in a classical system, where a relative phase between the bipartite is the key concept for the quantum feature of anticorrelation [25–29]. In this theory, the so-called HOM dip is supposed to be sinusoidally modulated as a function of the phase difference between two input photons within coherence time, where the conventional post-measurements are rather a minor process due to much delicate or sensitive phase effect on coherence as presented in Franson-type nonlocal correlation [11]. The Franson-type nonlocal correlation between remote bipartite entities has also been understood in terms of coupled coherence



physics between noninteracting MZIs via coincidence detection [27]. Finally, a coherence version of PBW [28] has been proposed recently under the name of coherence de Broglie waves (CBW) in an asynchronously coupled double Mach-Zehnder interferometer (ACD-MZI) system to demonstrate coherence optics-based quantum features applicable to quantum sensing and quantum metrology [36–43].

Very recently, CBW has been experimentally demonstrated in a pure classical regime of the ACD-MZI [29], where MZI has been implemented as a quantum device as discussed already for anticorrelation [25] and Franson-type nonlocal correlation [27]. Here, a general analysis of CBW is presented to give a better understanding of how such a nonclassical feature can be created in a pure classical system of MZIs. For this, quantum superposition between two paths of an MZI is investigated in a coupled system, where higher order phase-basis creation plays a major role. Here, we demonstrate that higher order phase bases are the origin of quantum features in CBW. This quantum feature is generated from the asymmetric coupling among MZIs which cannot be obtained by any classical means such as many-wave interference in cavity optics. Furthermore, a cavity CBW [37] is also investigated for potential applications of coherence quantum sensing such as inertial navigation [38, 39] and quantum lithography [40–43]. Here, the cavity CBW is also compared with an optical cavity to present their difference in fundamental physics.

## 2. Results

### 2.1. Analytical approach

Figure 1 shows a schematic of the coupled ACD-MZI for CBWs in reference [28]. Here, ACD is an asymmetrical phase relation between consecutive MZIs as indicated by the position of  $\varphi$ , where the phase  $\varphi$  represents either 0 or  $\pi$  phase shift between two paths of each MZI. To satisfy multiply coupled MZIs, the subscript  $q$  should be greater than one, which is a classical limit. For the phase basis of a single MZI, we redefine it from  $\{0, \pi\}$  to  $\{0, \varphi\}$  for simplicity. The multiply coupled MZI system in figure 1 is analyzed with an  $q$ -ordered tensor matrix notation of the phase bases for  $\psi = 0$ , where the  $\pi$ -basis of  $\psi$  induces a  $\pi$ -phase shift in the path superposition, resulting in breakage of the asymmetric coupling [28]:

In equation (1),  $q$  stands for the order of each MZI. Thus, the output of the  $q$ -coupled MZI system of figure 1 has  $2^q$  combinations with  $(1 + q)$  phase bases in terms of  $\varphi^j (j = 0, 1, 2, \dots, q)$ . Because the phase  $\varphi$  applies to the exponent of harmonic waves, the output field's phase can be represented by  $e^{iq\varphi_j} (j = 0, 1, 2, \dots, q)$ . In other words, the output phase basis varies along with  $q$ , where the fundamental  $\varphi$  bases are uniformly synchronized for all MZIs. Thus, the phase of the  $\varphi^q$  basis in equation (1) is represented by  $\varphi^q = (\pi/q) m$ , where  $m \leq q$ .

$$\begin{bmatrix} 0 \\ \varphi \\ \vdots \\ \varphi^q \end{bmatrix}_{q \times 1} = \begin{bmatrix} 0 \\ \varphi \end{bmatrix}_1 \otimes \begin{bmatrix} 0 \\ \varphi \end{bmatrix}_2 \cdots \otimes \begin{bmatrix} 0 \\ \varphi \end{bmatrix}_q. \quad (1)$$

To understand the coupled MZI system of figure 1, equation (1) is investigated with ordered bases of  $\varphi^q$  as follows:

(a) For  $q = 2$  in a doubly coupled MZI

$$\begin{bmatrix} 0 \\ \varphi \end{bmatrix}_1 \otimes \begin{bmatrix} 0 \\ \varphi \end{bmatrix}_2 = \begin{bmatrix} 0 \\ \varphi \\ \varphi \\ \varphi^2 \end{bmatrix}. \quad (2)$$

In a doubly coupled MZI system, the phase of the  $q$ th ordered basis is simply  $\varphi/q$  due to superposition in the output fields as  $(e^{i\varphi})^q$ . Thus, equation (2) implies CBW [28], whose eigenstates are  $\varphi^2$ ,  $\varphi$ , and 0.

We now define the basic building block of the ACD-MZI scheme for  $q = 2$  in figure 1 (see both blue and green boxes):

$$\begin{aligned} \begin{bmatrix} E_A \\ E_B \end{bmatrix} &= [-M] [\Psi] [M] \begin{bmatrix} E_0 \\ 0 \end{bmatrix}, \\ &= \frac{1}{4} \begin{bmatrix} (1 - e^{-i\varphi})(1 - e^{i\varphi}) - e^{i\psi}(1 + e^{-i\varphi})(1 + e^{i\varphi}) & i[(1 - e^{-i\varphi})(1 + e^{i\varphi}) - e^{i\psi}(1 - e^{i\varphi})(1 + e^{-i\varphi})] \\ i[(1 - e^{i\varphi})(1 + e^{-i\varphi}) - e^{i\psi}(1 - e^{-i\varphi})(1 + e^{i\varphi})] & -(1 + e^{-i\varphi})(1 + e^{i\varphi}) + e^{i\psi}(1 - e^{-i\varphi})(1 - e^{i\varphi}) \end{bmatrix} \begin{bmatrix} E_0 \\ 0 \end{bmatrix}, \end{aligned} \quad (3)$$

where  $[-M] = [\text{BS}] [-\varphi] [\text{BS}]$ ,  $[M] = [\text{BS}] [\varphi] [\text{BS}]$ ,  $[\text{BS}] = \frac{1}{\sqrt{2}} \begin{bmatrix} 1 & i \\ i & 1 \end{bmatrix}$ ,  $[\varphi] = \begin{bmatrix} 1 & 0 \\ 0 & e^{i\varphi} \end{bmatrix}$ ,  $[-\varphi] = \begin{bmatrix} 1 & 0 \\ 0 & e^{-i\varphi} \end{bmatrix}$ , and  $[\Psi] = \begin{bmatrix} 1 & 0 \\ 0 & e^{i\psi} \end{bmatrix}$ . Because CBW in figure 1 is based on coherence optics, the input field  $E_0$  is a classical field of any laser light. To solve equation (3), two different values of the  $\psi$ -bases are separately considered:

(a) For  $\psi = 0$ ,

Equation (3) is rewritten as:

$$\begin{bmatrix} E_A \\ E_B \end{bmatrix} = (-1) \begin{bmatrix} \cos(\varphi) & \sin(\varphi) \\ -\sin(\varphi) & \cos(\varphi) \end{bmatrix} \begin{bmatrix} E_0 \\ 0 \end{bmatrix}, \quad (4)$$

The corresponding intensities are as follows, respectively:

$$I_A = \frac{1}{2} [1 + \cos(2\varphi)] I_0, \quad (5)$$

$$I_B = \frac{1}{2} [1 - \cos(2\varphi)] I_0, \quad (6)$$

where  $I_j = E_j E_j^*$ . equations (5) and (6) show the lowest order of CBW in ACD-MZI [28, 29]. To briefly explain CBW, the basic building block in figure 1 is for  $q = 2$  corresponding to  $n = 1$ , where  $n$  represents the number of the basic building blocks of ACD-MZI. For  $n \geq 1$ , the following relation is obtained straightforwardly from equation (4) by matrix multiplications:

$$\begin{bmatrix} E_C \\ E_D \end{bmatrix}^n = (-1)^n \begin{bmatrix} \cos(n\varphi) & \sin(n\varphi) \\ -\sin(n\varphi) & \cos(n\varphi) \end{bmatrix} \begin{bmatrix} E_0 \\ 0 \end{bmatrix}. \quad (7)$$

Thus, the phase resolution of the output fields linearly increases with respect to  $n$ . Without doubt, this kind of resolution enhancement can be obtained from multi-wave interference in classical cavity physics without superposition among each bipartite system of MZIs in figure 1 (discussed in figures 2 and 3). In other words, CBW in equation (7) has an effect of PBS, while the classical cavity optics does not (discussed in figure 3). The corresponding intensities are as follows, respectively:

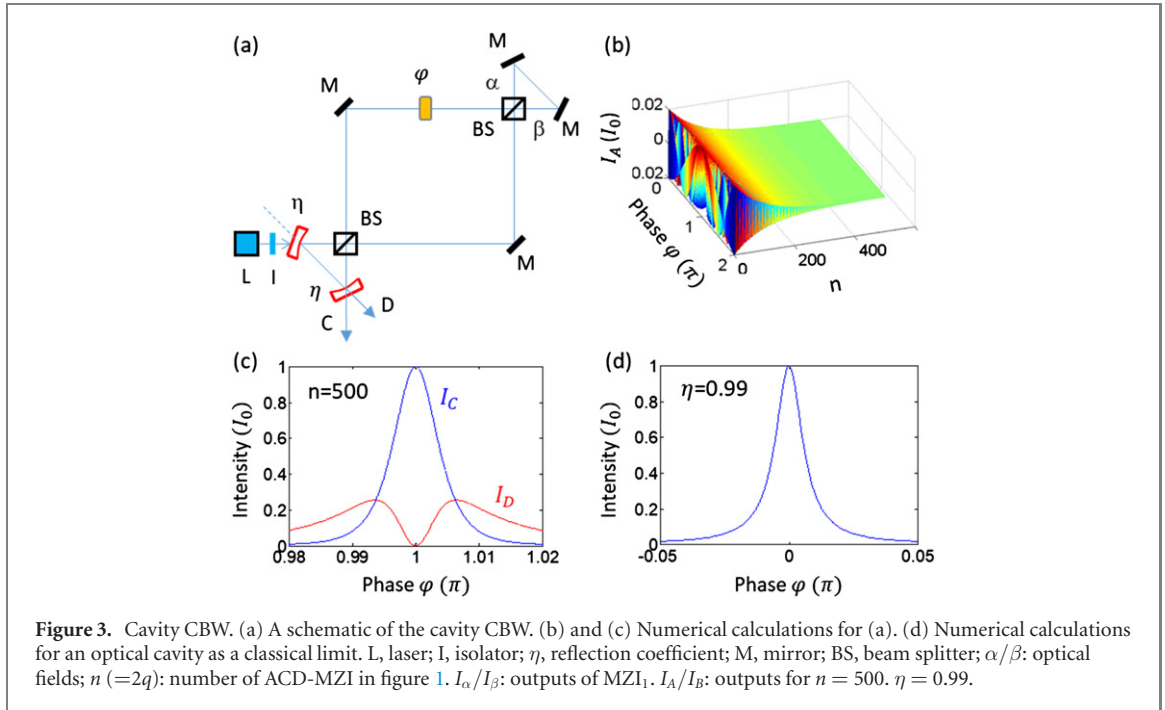
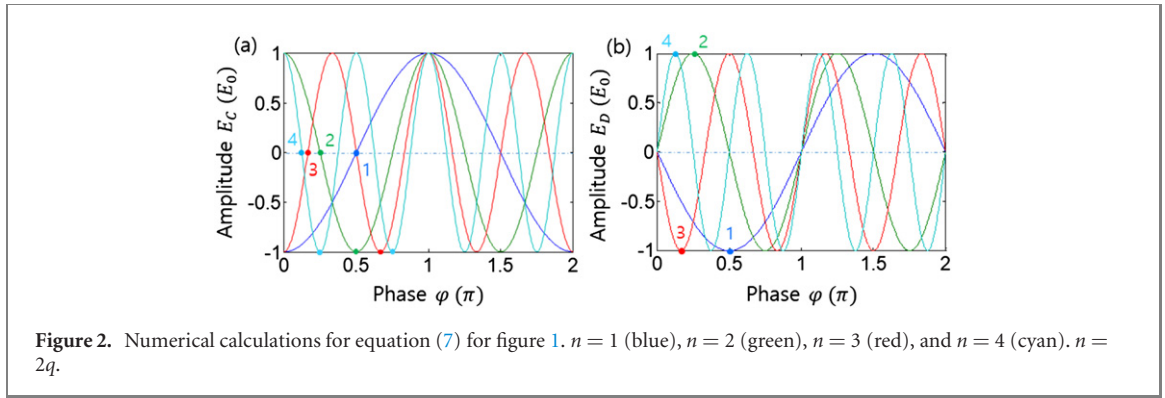
$$(I_C)^n = I_0 \cos^2 n\varphi, \quad (8)$$

$$(I_D)^n = I_0 \sin^2 n\varphi. \quad (9)$$

(b) For  $\psi = \pi$

$$\begin{bmatrix} E_C \\ E_D \end{bmatrix} = \begin{bmatrix} 1 & 0 \\ 0 & 1 \end{bmatrix} \begin{bmatrix} E_0 \\ 0 \end{bmatrix}. \quad (10)$$

Equation (10) is for the case of unconditionally secured classical key distribution (USCKD) as an identity relation between the input and output [26]. This identity relation is the same as the



$\varphi$ -symmetric case with  $\psi = 0$  [see section 1 of the supplementary information (<https://stacks.iop.org/NJP/22/123043/mmedia>)]. For the tensor notation in equations (2) and (10) is represented as:

$$\begin{bmatrix} 0 \\ \varphi \end{bmatrix}_1 \otimes \begin{bmatrix} 0 \\ -\varphi \end{bmatrix}_2 = \begin{bmatrix} 0 \\ -\varphi \\ \varphi \\ 0 \end{bmatrix}, \quad (11)$$

where the ‘-’ sign of  $\varphi$  in equation (11) is due to the  $\pi$ -phase shift by the control phase  $\psi$  in figure 1. Like equations (10) and (11) also shows the identity relation with the same phase bases. Here, the sign in equations (4) and (11) does not alter the intensity. Although two different cases of (a) and (b) result in distinctly different outputs, they root in the same physics of nonclassical CBW, but represent quantum and classical features, respectively, where the identity relation is an extreme case of CBW without superposition between MZIs [29]; this will be discussed in figure 2.

To investigate ACD-MZI in figure 1 for the ordered phase bases, equation (2) needs to be redefined as:

$$\begin{bmatrix} 0 \\ \varphi \\ \varphi \\ \varphi^2 \end{bmatrix} \rightarrow (1, 2, 1), \quad (12)$$

where each element in the parenthesis of (1, 2, 1) represents corresponding coefficient of the ordered phase basis of  $(\varphi^0, \varphi^1, \varphi^2)$  in terms of probability. From the reference bases of 0 and  $\pi$  in a single MZI, equation (12) shows three possible bases, where  $\varphi^1$  indicates the reference basis. Because the phase

**Table 1.** The number of MZI ' $q$ ' vs the phase order ' $\varphi^q$ ' of the output fields in equation (1).

$q$	$\varphi^q$							
	0	1	2	3	4	5	6	7
2	1	2	1					
3	1	3	3	1				
4	1	4	6	4	1			
5	1	5	10	10	5	1		
6	1	6	15	20	15	6	1	
7	1	7	21	35	35	21	7	1

basis  $\varphi^2$  relates with  $e^{i2q}$ ,  $\varphi^2 = (\pi/2) m$  ( $m \leq 2$ ) is achieved. Thus, the phase basis set of  $\varphi^2$  is represented as  $\varphi^2 \in \{0, \frac{\pi}{2}, \pi\}$ . As a result, the  $q$ th ordered phase basis is represented as:

$$\varphi^q = (\pi/q) m \quad (m \leq q), \quad (13)$$

where  $m \leq q$ . Thus, the phase basis in a coupled system is given:

$$\varphi^q \in \left\{ 0, \frac{\pi}{q}, \frac{2\pi}{q}, \dots, \frac{(q-1)\pi}{q}, \pi \right\}, \quad (14)$$

where, the number of phase bases for  $q$ -coupled MZIs is  $q + 1$ . Here, it should be noted that the lowest phase basis  $\pi/q$  represents the fundamental basis of the  $q$ -coupled MZI system. The general notation for coefficients of the phase bases in equation (14) for higher  $q$  represents the Pascal's triangle as shown in table 1 (see section 2 of the supplementary information). Here, the lowest phase basis represents CBW in an asymmetric structure of MZIs of figure 1, in which CBW corresponds to a N00N state in the particle nature of entangled photons.

For the  $q$ th ordered phase basis of  $\varphi^q$ , the output field's intensity has a sinusoidal oscillation in the form of  $e^{i\varphi^q}$ . Thus, the phase basis of  $\varphi^q = (\pi/q) m$  is successfully summarized in table 1. The increased phase bases, of course, result in a  $q$ -times enhanced phase resolution applicable to quantum sensing. As a result, the effective wavelength of CBW is  $\lambda_{\text{CBW}} = \lambda_0/2q$ , corresponding to that of PBW in  $\lambda_{\text{PBW}} = \lambda_0/4N$ , where  $N$  is the number of entangled photons on a BS. The 1/2 ratio between CBW and PBW is due to the  $g^{(1)}$  correlation in CBW over the  $g^{(2)}$  (intensity) correlation in PBW. Considering the  $g^{(2)}$  (intensity) correlation in CBW,  $q$  functions as  $N$ . Thus, the coupling effect of a tensor matrix in equation (2) has been demonstrated for the  $q\varphi$  phase oscillation, resulting in a  $q$ -times enhanced phase resolution in the output fields [17–20, 28, 29, 35, 36]. On the contrary, the benefit of  $g^{(2)}$  in the coincidence detection for entangled photon pairs based on the probabilistic nature of photons, the present case of CBW is deterministic based on the wave nature of photons, resulting in no need of the coincidence detection due to the long coherence time by definition of the wave nature and high signal to noise ratio.

## 2.2. Numerical approach

Figure 2 shows numerical calculations for  $E_C$  for a few different  $n$  ( $=2q$ ), where  $n$  is the number of basic building block of MZIs satisfying ACD-MZI in figure 1 for  $\psi = 0$ . As  $n$  increases, the fundamental phase  $(\pi/q)$  of  $\varphi^q$  inversely proportional to  $q$  as shown in figure 2 (see the colored dots). Here, the fundamental basis phase  $\varphi^q$  is obtained from the maximum output intensity. Due to alternative sign modulations in equation (7), the superposed fields for all  $E_C$  and  $E_D$  becomes zero, except  $\varphi = \pm\pi$  in figure 2(a) (see section 3 of the supplementary information). Thus, the tensor analysis in the coupled MZI system strongly supports the origin of nonclassicality in terms of newly generated phase bases in  $e^{i\varphi^q}$  harmonic waves. This quantum feature of  $\lambda_{\text{CBW}} = \lambda_0/2q$  is created from purely coherence optics via macroscopic coupling of the path superposition among MZIs in figure 1.

Instead of the serial connection of the two-mode MZIs in figure 1 for CBW as denoted in table 1, the recursive structure of figure 1 can be obtained for a cavity CBW. Figure 3(a) shows a schematic of a cavity CBW, where the asymmetric phase relation between consecutive MZIs are satisfied for all recursive fields. Figure 3(b) shows the corresponding numerical calculations as functions of  $\varphi$  and  $n$ , where the reflection coefficient  $\eta$  is set at 0.99. The control phase  $\psi$  is set to zero automatically and precisely due to the shared paths located at both ends of the bow-tie structure. The alternative sign change among the ordered fields' amplitudes of  $E_C$  in equation (7) results in a complete cancellation of the output fields due to superposition for all phases except for  $\varphi = \pm\pi$  for  $I_C$  if  $n \gg 1$  as mentioned in figure 2 (see figure 3(c)). Even with reflectance  $R$  ( $=\eta^2$ ) of the output coupler, the gradual intensity decrease in the bounced fields, however, does not affect the overall fields' cancellation (see section 3 of the supplementary information). Unlike  $E_C$ ,

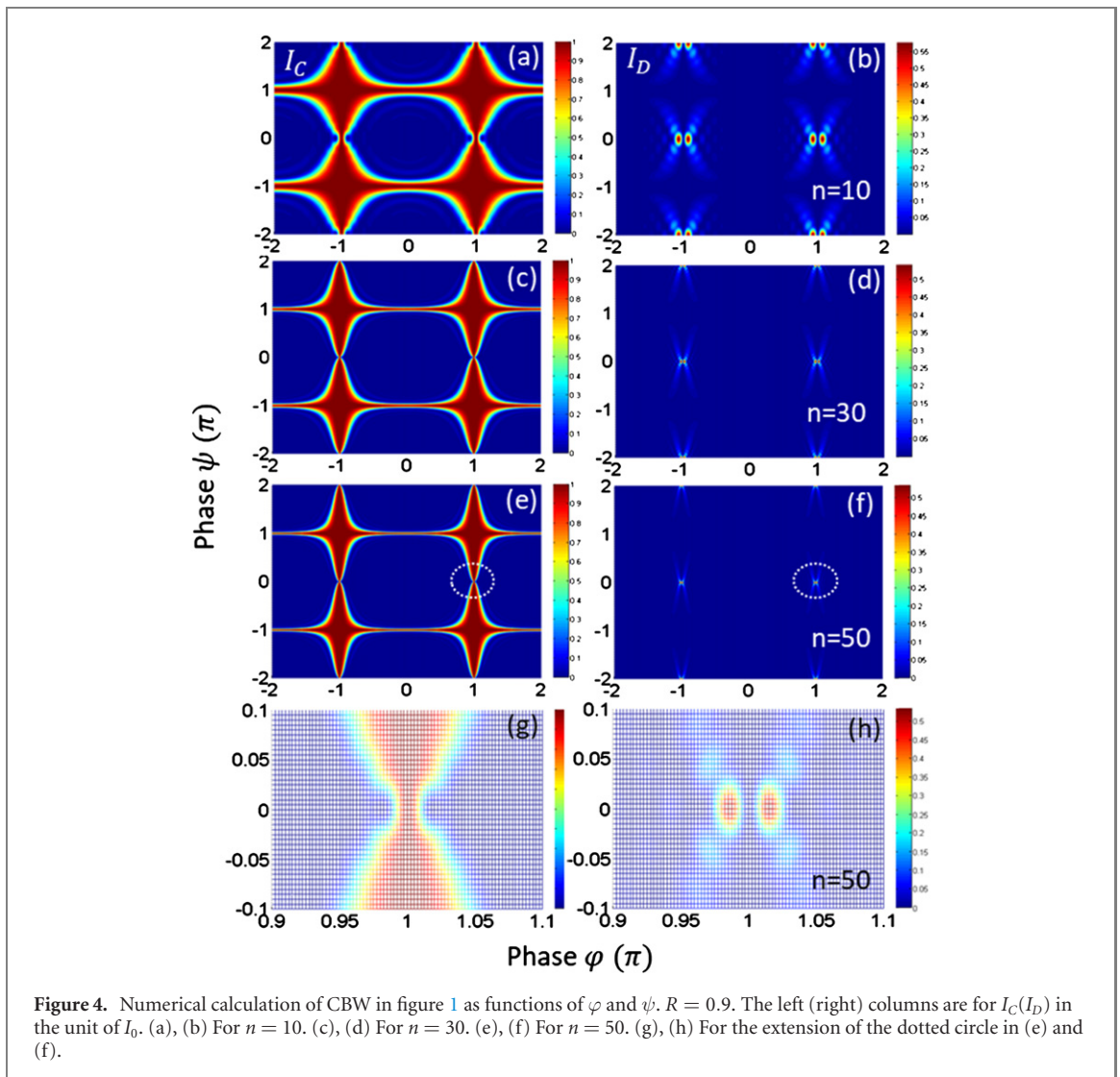


**Figure 4.** Numerical calculation of CBW in figure 1 as functions of  $\varphi$  and  $\psi$ .  $R = 0.9$ . The left (right) columns are for  $I_C$  ( $I_D$ ) in the unit of  $I_0$ . (a), (b) For  $n = 10$ . (c), (d) For  $n = 30$ . (e), (f) For  $n = 50$ . (g), (h) For the extension of the dotted circle in (e) and (f).

however,  $E_D$  experiences a destructive interference at  $\varphi = \pi$ , resulting in zero in intensity [see the red curve in figure 3(c)], where these interference patterns repeat at  $\varphi = \pm(2n - 1)\pi$  [28].

The intensity and phase resolution of  $I_C$  and  $I_D$  at  $\varphi = \pm\pi$  are higher than the classical counterpart as shown in figure 3(d), where figure 3(d) is for a typical Fabry–Perot (FP) interferometer as a reference (see chapter 8 of reference [1]). Here, it should be noted that the physics of enhanced phase resolution in figures 3(c) and (d) is completely different from each other, where the classical one in figure 3(d) is due to the superposition of reflected fields in FP, in which each reflected field has a different phase due to different cavity round-trip distance for the same wavelength [1]. On the contrary, the enhanced phase resolution in figure 3(c) is due the quantum feature of CBWs based on equations (7) and (13). Figure 3(a) has already been applied for CBW Sagnac interferometer in a modified scheme [37], where the highly sensitive phase resolution can be used for inertial navigation without the help of the global positioning system.

The spectrum of  $I_C$  in figure 3(c) is quite different from that of an optical cavity FP interferometer, where both constructive and destructive interferences occur at  $\varphi = \pm\pi$  with a modulus of  $2\pi$ . On the contrary, the FP interferometer shows constructive interference at  $\varphi = 2p\pi$  ( $p = 0, 1, 2, \dots$ ) as shown in figure 3(d), whose spectral width is proportional to  $\eta$ -based finesse. Although both cavity CBW and FP are based on many-wave interference, the origin of CBW is nonclassical with  $\lambda_{\text{CBW}} (= \frac{\lambda_0}{2q}m)$  via asymmetric coupling among MZIs, while FP is given by the cavity length-dependent resonance condition. Thus, cavity CBWs interfere with self-generated  $q$ -dependent wavelengths in the cavity, while FP induces no change in the input frequency of light. For a fixed  $\eta$ , the spectral width of  $I_C$  in figure 3(c) is 67% narrower than that of FP in figure 3(d). A high-resolution spectrometer based on figure 3 can also be implemented using silicon waveguides of the serial MZI structure of figure 1 [7, 44, 45].

Figure 4 shows numerical calculations for the output fields as functions of  $\varphi$  and  $\psi$  of ACD-MZIs. Both phases have the same modulus of  $2\pi$ . From the top to the bottom the number  $n$  increases. As mentioned above the control phase  $\psi$  functions as a toggle switch between CBW and USCKD depending on the choice of its basis. The phase sensitivity increases as  $n$  increases. Figures 4(g) and (h) extensions of figures 4(e) and (f), where the width of  $0.02\pi$  is confirmed in both  $\varphi$  and  $\psi$ . As shown in the lower right corner, the output intensity  $I_D$  is quite sensitive to the phase variance of both  $\varphi$  and  $\psi$ . As mentioned above in figure 3, the round trip number  $n$  in the cavity CBW is much bigger than 50 even with  $R = 0.9$ . Thus, the CBW sensitivity is much higher than that of optical cavity relying on finesse [1]. Most of all, the variance of  $\psi$  is zero due to the shared path in the bow-tie structure of figure 3 in an ideal condition. The phase noise of  $\varphi$  can also be maintained to be nearly zero such as in the silicon waveguide structure whose refractive index varies by temperature only [45].

### 3. Discussion

Unlike conventional nonclassical feature based on the particle nature of photons such as N00N state-based PBW, CBW is based on multi-superposition between macroscopic MZIs via an asymmetric coupling method. As is well known, coherence as a wave nature does rather rely on ‘phase’ than ‘photon number’ according to the Heisenberg’s uncertainty principle. Compared with that the photon loss is critical to PBW due to the particle nature of individual photons, the diminution of nonclassical feature in CBW is due mostly to coherence loss between MZIs via phase variation. In other words, the phase uncertainty in  $\varphi$  and  $\psi$  is critical to maintain quantumness of the present CBW system as shown in figure 4.

### 4. Conclusion

In conclusion, a nonclassical feature of CBWs is analyzed using tensor matrices of binary basis systems of MZI. Analyzing a coupled MZI system using both phase basis tensor matrices and numerical calculations, the origin of the nonclassical properties of CBWs was demonstrated for the  $n$ th order phase basis whose phase resolution is  $n$ -times enhanced compared with the classical diffraction limit. The number of phase bases in an ACD-MZI system was also demonstrated and resulted in Pascal’s triangle. For potential applications of CBWs, cavity CBWs were also analyzed for enhanced phase resolution even with low finesse cavity. Although the output mode looks similar to the conventional optical cavity mode, its physics is completely different, satisfying nonclassical physics. For potential applications, silicon photonics may be a good tool to implement cavity CBWs with even low finesse.

### Acknowledgments

BSH acknowledges that the present research was supported by a GRI Grant of GIST 2020.

### ORCID iDs

Byoung S Ham  <https://orcid.org/0000-0003-3609-8508>

### Reference

- [1] Pedrotti F L, Pedrotte L and Pedrotte L S 2007 *Introduction to Optics* 3rd edn (New York: Pearson Education)
- [2] Hong C K, Ou Z Y and Mandel L 1987 *Phys. Rev. Lett.* **59** 2044
- [3] Kaltenbaek R, Blauensteiner B, Zukowski M, Aspelmeyer M and Zeilinger A 2006 *Phys. Rev. Lett.* **96** 240502
- [4] Santori C, Fattal D, Vučković J, Solomon G S and Yamamoto Y 2002 *Nature* **419** 594
- [5] Ou Z Y and Mandel L 1988 *Phys. Rev. Lett.* **61** 54
- [6] Valencia A, Scarcelli G, D’Angelo M and Shih Y 2005 *Phys. Rev. Lett.* **94** 063601
- [7] Paesani S, Borghi M, Signorini S, Mainos A, Pavesi L and Laing A 2020 *Nat. Commun.* **11** 2505
- [8] Peruzzo A, Shadbolt P, Brunner N, Popescu S and O’Brien J L 2012 *Science* **338** 634
- [9] Lettuo R, Rezus Y L A, Renn A, Zumofen G, Ikonen E, Gotzinger S and Sandoghdar V 2010 *Phys. Rev. Lett.* **104** 123605
- [10] Deng Y-H *et al* 2019 *Phys. Rev. Lett.* **123** 080401
- [11] Franson J D 1989 *Phys. Rev. Lett.* **62** 2205
- [12] Kwiat P G, Steinberg A M and Chiao R Y 1993 *Phys. Rev. A* **47** R2472
- [13] Brendel J, Gisin N, Tittel W and Zbinden H 1999 *Phys. Rev. Lett.* **82** 2594
- [14] Franson J D 2010 *Science* **329** 396
- [15] Jogenfors J, Elhassan A M, Ahrens J, Bourennane M and Larsson J-Å 2015 *Sci. Adv.* **1** e1500793
- [16] Horn M A, Shimony A and Zeilinger A 1989 *Phys. Rev. Lett.* **62** 2209

- [17] Jacobson J, Björk G, Chuang I and Yamamoto Y 1995 *Phys. Rev. Lett.* **74** 4835
- [18] Walther P, Pan J-W, Aspelmeyer M, Ursin R, Gasparoni S and Zeilinger A 2004 *Nature* **429** 158
- [19] Xiao M, Wu L-A and Kimble H J 1987 *Phys. Rev. Lett.* **59** 278
- [20] Wang X-L *et al* 2018 *Phys. Rev. Lett.* **120** 260502
- [21] Kim H, Lee S M, Kwon O and Moon H S 2017 *Sci. Rep.* **7** 5772
- [22] Solano E, de Matos Filho R L and Zagury N 1999 *Phys. Rev. A* **59** R2539
- [23] Grangier P, Roger G and Aspect A 1986 *Europhys. Lett.* **1** 173
- [24] Greenberger D M, Horne M A and Zeilinger A 1993 *Phys. Today* **46** 22
- [25] Ham B S 2020 *Sci. Rep.* **10** 7309
- [26] Ham B S 2020 *Sci. Rep.* **10** 11687
- [27] Ham B S 2020 The origin of correlation fringe in Franson-type experiments (arXiv:2005.14432)
- [28] Ham B S 2020 *Sci. Rep.* **10** 12899
- [29] Ham B S 2020 Observation of coherence de Broglie waves (arXiv:2007.04738)
- [30] Schrödinger E 1935 *Naturwissenschaften* **23** 823
- [31] Friedman J R, Patel V, Chen W, Tolpygo S K and Lukens J E 2000 *Nature* **406** 43
- [32] Monore C, Meekhof D M, King B E and Wineland D J 1996 *Science* **272** 1131
- [33] Vedral V 2008 *Nature* **453** 1004
- [34] Julsgaard B, Kozhekin A and Polzik E S 2001 *Nature* **413** 400
- [35] Muller-Ebhardt H, Rehbein H, Schnabel R, Danzmann K and Chen Y 2008 *Phys. Rev. Lett.* **100** 013601
- [36] Degen C L, Reinhard F and Cappellaro P 2017 *Rev. Mod. Phys.* **89** 035002
- [37] Ham B S 2020 Coherently driven quantum metrology using a photonic de Broglie Sagnac interferometer (arXiv:2002.01753)
- [38] Khial P P, White A D and Hajimiri A 2018 *Nat. Photon.* **12** 671
- [39] Geiger R *et al* 2012 *Nat. Commun.* **2** 474
- [40] Boto A N, Kok P, Abrams D S, Braunstein S L, Williams C P and Dowling J P 2000 *Phys. Rev. Lett.* **85** 2733
- [41] D'Angelo M, Chekhova M V and Shih Y 2001 *Phys. Rev. Lett.* **87** 013602
- [42] Liao Z, Al-Amri M and Zubairy M S 2010 *Phys. Rev. Lett.* **105** 183601
- [43] Hemmer P R, Muthukrishnan A, Scully M O and Zubairy M S 2006 *Phys. Rev. Lett.* **96** 163603
- [44] Sibson P, Kennard J E, Stanisic S, Erven C, O'Brien J L and Thompson M G 2017 *Optica* **4** 172
- [45] Elshaari A W, Pernice W, Srinivasan K, Benson O and Zwiller V 2020 *Nat. Photon.* **14** 285